THE PENNSYLVANIA STATE UNIVERSITY
SCHREYER HONORS COLLEGE

DEPARTMENTS OF MATHEMATICS AND ASIAN STUDIES

TIME-SPLITTING SINE SPECTRAL METHODS FOR SIMULATING FEMTOSECOND LASER PROPAGATION

MATTHEW STEIN
Summer 2010

A thesis
submitted in partial fulfillment
of the requirements
for baccalaureate degrees
in Mathematics, Chinese, and International Studies
with interdisciplinary honors in Mathematics and Chinese

Reviewed and approved* by the following:

Xiantao Li
Asst Prof of Mathematics
Thesis Supervisor

Andrew Belmonte
Assoc Prof of Mathematics
Honors Adviser

Shuang Shen
Asst Prof CMPLT/ASIAN ST
Honors Adviser

* Signatures are on file in the Schreyer Honors College.

ABSTRACT 摘要

The goal of this project was to make a better approximation of the propagation of the femtosecond laser. Our eventual goal was to provide a model on the kilometer scale, which would enable long-range atmospheric sensing, namely of particulates. In this paper only short ranges were tested. After analyzing the model and establishing its effectiveness, beams with different parameters, initial conditions, and combinations were investigated. The goal was to take the existing work, apply a different method of integration (third order time-splitting sine-spectral method), and get a model more stable at longer ranges. The model is exponential order in mesh size, first order in time step size.

这个项目的目的是形成 一个比较好的飞秒激光船舶的近似。我们的最后的目的是建立能做长距离大气候传感的公里规模的模型。即空气中悬浮微粒。在这个报告中，我们只进行了短距离测试。我们的目标是利用已有的知识，使用别的积分方法（三阶时间分步正弦谱法），最终形成在长距离也比较稳定的模型。到底这个模型网距指数收敛，时间步距一阶收敛。

Table of Contents

ACKNOWLEDGEMENTS

I would like to thank the Institute of International Education and the Boren National Security Education Program for funding my final year of study at National University of Singapore. I would like to thank the National University of Singapore - where this project took place, Professor Weizhu Bao – my advisor at NUS, Xuanchun Dong – my primary advisor, and Ganzali for the kindness and computer help. I'd like to thank as well Dr. Tineke Cunning helping me win the Boren Scholarship, Susan Knell, Roberta Hardin, Mrs. Patricia Schulte, James Sellers, and Julianna Chaszar for their patience and extra hours of assistance.

1 INTRODUCTION 入门

This is a nonlinear optics problem that can be modeled by the damped nonlinear Schrodinger wave equation. Femtosecond lasers are commonly used in sensing and in manufacturing. Currently, they are used at short ranges, on or below the meter scale. Extensive work has been done in obtaining weights and parameters determining the significance of the terms representing atmospheric and physical effects on the beam. Vincotte's χ^5 susceptibility term was included in the model [3].

这个非线性光学的问题可用非线性阻尼的雪定额（Schrodinger）波动方程建模研究。飞秒激光平常使用于生产和传感。现在，它大部分被短程使用，单位为米或更小。人们做了很多研究来决定影响这种激光的大气和物理效应的参数。模型也包括 Vincotte's χ5 敏感度[3]。

2 MATHEMATICAL MODELING PROCEDURE 数学模拟方法

2.1 The 3D physical model 3D物质模型

The 3D model is most directly analogous to the physical world. It is governed by the below equation:

3D模型跟物质世界最同的。下方程描述：

$$\frac{\partial \mathcal{E}(x,y,z,t)}{\partial z} = \frac{i}{2k_0}\nabla_\perp^2 \mathcal{E} + ik_o\left(n_2\mathcal{R}(t) - n_4|\mathcal{E}|^4\right)\mathcal{E} - i\frac{k''}{2}\frac{\partial^2}{\partial t^2}\mathcal{E} - \left(\frac{ik_0}{2\rho_c} + \frac{\sigma}{2}\right)\rho\mathcal{E} - \frac{\beta^{(K)}}{2}|\mathcal{E}|^{2K-2}\mathcal{E}, \tag{2.1}$$

$$\mathcal{R}(t) = \frac{1}{2}\left(|\mathcal{E}|^2 + \tau_K^{-1}\int_{-\infty}^{t} e^{-\frac{t-t'}{\tau_K}}|\mathcal{E}(t')|^2 \mathrm{d}t'\right), \quad (x,y,z)\in\mathbb{R}^3, \quad t>0, \tag{2.2}$$

$$\frac{\partial \rho(x,y,z,t)}{\partial t} = \sigma_K \rho_{\mathrm{nt}}|\mathcal{E}|^{2K} + (\sigma/U_i)\rho|\mathcal{E}|^2, \tag{2.3}$$

where E is the electric field envelope, $\rho(x,y,z,t)$ is the free electron density excited by ionization of air molecules and z is the direction of propagation. These equations discount high-order dispersion and space-time focusing and self-steepening because the pulse duration used in this study ($t_p = 250$ fs) is sufficiently long. The $\nabla_\perp^2\mathsf{E}$ term is the diffraction in the x and y directions, ω_0 is the carrier wave frequency, λ_0 is the wavelength and in this case $\lambda_0 = 800nm$, and $k_0 = \omega_0/c$. The second is Kerr focusing term, where n_2 is Kerr refraction index, in this case, $n_2 = 4\times10^{-19}cm^2/W$. $\mathsf{R}(t)$ is complete Kerr response of air, taking into account both instantaneous and delayed responses, $ik_o n_2|\mathsf{E}|^2\mathsf{E}$ being the instantaneous Kerr

refraction (cubic and linear), $ik_0 n_2 \tau_K^{-1} \int_{-\infty}^{t} e^{-\frac{t-t'}{\tau_K}} |\mathrm{E}(t')|^2 \, \mathrm{d}t' \mathrm{E}/2$ is the delayed Kerr refraction (cubic and linear), and $ik_0 n_4 |\mathrm{E}|^4 \mathrm{E}$ being the quintic Kerr refraction response to air, where τ_K is the relaxation time, in this case $\tau_K = 70\,fs$, n_4 is the quintic saturation coefficient, $n_4 = 2.5\times10^{-33} cm^4/W^2$. $i\frac{k''}{2}\frac{\partial^2}{\partial t^2}\mathrm{E}$ is the group velocity dispersion (GVD) term, which insures dispersion in the time (temporal) direction, where $k'' = 0.2\,fs^2/cm$. This term is important and will have to be eliminated when going from 3D model to the 2D model. The $\sigma\rho\mathrm{E}/2$ is the plasma defocusing from oxygen ionization, ρ_c is the critical plasma density, beyond which the beam cannot propagate ($\rho_c = 1.8\times10^21 cm^{-3}$). $\frac{\beta^{(K)}}{2}|\mathrm{E}|^{2K-2}\mathrm{E}$ is the multiphoton absorption (MPA) term, ensuring power dissipation, with $\beta^{(K)} = 3.1\times10^{-98} cm^{2K-3}/W^{K-1}$. $\frac{\partial\rho(x,y,z,t)}{\partial t}$ change in plasma density over time. This is where plasma defocusing is accounted for. $\sigma_K \rho_{nt} |\mathrm{E}|^{2K}$ is multiphoton ionization where $\rho_{nt} = 5.4\times10^{18} cm^{-3}$, neutral density of oxygen molecules, and $\sigma_K = 2.9\times10^{-99} s^{-1}\, cm^{2K}/W^K$, the coefficient of multiphoton ionization and K is the number of photons involved. In this case, eight photons are needed to extract electrons from such neutral density oxygen molecules. σ is the coefficient of avalanche (cascade) ionization and plasma absorption from cross section for inverse bremsstrahlung $\sigma = 5.4\times10^{-20} cm^2$. $(\sigma/U_i)\rho|\mathrm{E}|^2$ is the ionization of oxygen molecules' contribution to defocusing, where $U_i = 12.1eV$, the gap potential of oxygen molecules (O_2).

E 是电场包膜, $\rho(x,y,z,t)$ 是自由电子密度从空气分子离子化然后 z 是传播往.
这些方程不管告阶分散，宏时聚焦，和自陡结果/参数因为脉冲持续时间长够（$t_p = 250\,\mathrm{fs}$)。
$\lambda_0 = 800nm$, and $k_0 = \omega_0/c$. $\nabla_\perp^2\mathrm{E}$ 项是x,y往衍射， ω_0 是载波频， λ_0 是波长（现在 $\lambda_0 = 800nm$ ， $k_0 = \omega_0/c$ 。第二个项是克尔聚焦项， n_2 是克尔折光率， $n_2 = 4\times10^{-19} cm^2/W$ 。 $\mathrm{R}(t)$ 是完全空气克尔响应包括瞬态和延迟响应， $ik_o n_2 |\mathrm{E}|^2 \mathrm{E}$ 是顺泰克尔折光（一阶和三阶/一次方和三次方）， $ik_0 n_2 \tau_K^{-1} \int_{-\infty}^{t} e^{-\frac{t-t'}{\tau_K}} |\mathrm{E}(t')|^2 \, \mathrm{d}t' \tilde{A}\square\ \hat{A}/2$ 是延迟克尔折光（一和三次方/一三阶）， $ik_0 n_4 |\mathrm{E}|^4 \mathrm{E}$ 是五次方克尔折光空气响应， τ_K 是弛豫时间（ $\tau_K = 70\,fs$ ），n_4 是五次方饱和系数（ $n_4 = 2.5\times10^{-33} cm^4/W^2$ ）。 $i\frac{k''}{2}\frac{\partial^2}{\partial t^2}\mathrm{E}$ 是群组速度离差（波群速度折光）项，让分散在时间往， $k'' = 0.2\,fs^2/cm$ 。将来这项很重要，将来会从三维模型消除形成两维模型。$\sigma\rho\mathrm{E}/2$ 是氧气造成等离子体散焦。$\sigma\rho\mathrm{E}/2$ 是临界等离子体密度，比那个高激光传不播 $\rho_c = 1.8\times10^21 cm^{-3}$ 。 $\frac{\beta^{(K)}}{2}|\mathrm{E}|^{2K-2}\mathrm{E}$ 是多光子吸收项（MPA），让力驱散。

$\beta^{(K)} = 3.1\times10^{-98} cm^{2K-3}/W^{K-1}$。$\frac{\partial\rho(x,y,z,t)}{\partial t}$是等离子体密度跑时间。在这儿等离子体散焦计算。$\sigma_K \rho_{nt} |\mathsf{E}|^{2K}$ 是多光子电离，$\rho_{nt} = 5.4\times10^{18} cm^{-3}$，氧分子的中性密度，和 $\sigma_K = 2.9\times10^{-99} s^{-1}\ cm^{2K}/W^K$，是多光子电离的系数，和 K 是多少光子参加。一般来说，从中性密度的氧分子提取点子要求八个光子。σ 是雪崩电离和等离子吸收于非韧致辐射（bremsstrahlung）截面系数，$\sigma = 5.4\times10^{-20} cm^2$。$(\sigma/U_i)\rho|\mathsf{E}|^2$ 是分子氧离子的造成散焦的部分，$U_i = 12.1eV$，是分子氧(O_2)的空袭电位

2.2 A dimensionless 2D model 无尺寸的2维的模型

A 2D model was derived because the 3D model is too computationally expensive for the purposes of extending range, and a 2D model also allows for better viewing of each time step. Here, we refer to the procedures by A. Vincotte and L. Berge, 2006 [2]. Introducing dimensionless variables $z \to 4z_0 z$, $t \to t t_p$, $(x,y) \to (x,y)\omega_0$, $\mathsf{E} \to \sqrt{P_{cr}/4\pi\omega_0^2}$ and $\rho \to (\rho_c/2z_0k_0)\rho$, where $z_0 = \pi\omega_0^2/\lambda_0$ denotes the Rayleigh length for Gaussian beams ω_0 in waist. In making the 2D model, the Ansatz that the electric field envelope could be separated into a time-dependent Gaussian function and an independent spatial function (also Gaussian) allows:

因为 3 维的模型把扩展范围太打[为了]算的贵（用太多计算机资源），取得 2 维模型。2 维模型让检查个个时间步进。使用 Vincotte and L. Berge, 2006 [2] 的程序。介绍无尺寸的参数[变数]: $: z \to 4z_0 z$, $t \to t t_p$, $(x,y) \to (x,y)\omega_0$, $\mathsf{E} \to \sqrt{P_{cr}/4\pi\omega_0^2}$ 和 $\rho \to (\rho_c/2z_0k_0)\rho$, $z_0 = \pi\omega_0^2/\lambda_0$ 是高斯光束 ω_0 腰的瑞利长度。形成 2D 模型，透过如下前提/拟设：电场包络可分开到关于时间的高斯函数和不关于实空间的函数（也是高斯的）让[成了]:

$$\mathsf{E}(x,y,z,t) = \psi(x,y,z)\times e^{-[t-t_c(z)]^2/T^2}. \quad (1)$$

Plugging this Ansatz into (Eq 2)-(Eq 3), we end up with the following dimensionless 2D model for the spatial profile ψ :

透过如下前提在（方程2，方程3）,形成2D无尺寸模型于实空间波形 ψ :

$$i\partial_z\psi + \nabla_\perp^2\psi + f(|\psi|^2)\psi + i\nu|\psi|^{2K-2}\psi = 0, \quad (2)$$

$$f(|\psi|^2) = \alpha|\psi|^2 - \varepsilon|\psi|^4 - \gamma|\psi|^{2K}. \quad (3)$$

For its detailed derivation, we refer to [2]. The coefficients in the above equations are determined by the physical setting, e.g., for the case where duration $t_p = 250\,fs$, $\alpha = 0.446$, $\varepsilon = 7.3\times10^{-7} cm^2/\omega_0^2$, $\gamma = 8.4\times10^{-40} cm^{2(K-1)}/\omega_0^{2(K-1)}$ and $\nu = 1.2\times10^{-35} cm^{2(K-2)}/\omega_0^{2(K-2)}$, where ω_0 expressed in cm.

察看[2]为了全体的导出法．物质环境决定上方程的系数．比如说，持续时间是 $t_p = 250\,fs$ ， $\alpha = 0.446$ ， $\varepsilon = 7.3\times10^{-7} cm^2/\omega_0^2$ ， $\gamma = 8.4\times10^{-40} cm^{2(K-1)}/\omega_0^{2(K-1)}$ 和

$\nu = 1.2\times10^{-35} cm^{2(K-2)}/\omega_0^{2(K-2)}$, ω_0 是cm.

3 TIME-SPLITTING SINE SPECTRAL METHODS 时间分步正弦谱法

After deriving the 2D model, a spectral method was implemented for integrating the 2D equation. The time splitting sine spectral method developed in [1] was implemented. The second order method integrates in two steps: integrating the transversal term in phase space from z_n to z_{n+1} and using that value as initial data for integrating the remaining terms in real space from z_n to z_{n+1}; whereas the third order method integrates in three steps:

取得 2 D模型后，使用谱方法积分 2 D方程。使用[1]发展的时间分步正弦谱方法。2阶方法用 2 步进为了积分方程：第1：在横向项在相空间积分 z_n 到 z_{n+1}， 然后用该值作为初始值对剩余项从 z_n 到 z_{n+1} 进行积分；3阶积分方法有3个步进：

First, starting with initial data $\psi(x,y,z_0) = f(x,y)$, the transverse term is solved for exactly in one half time step using the discrete sine transform, integrating in phase space from ψ^* from (x,y,z_k) to $(x,y,z_{k+1/2})$, and then taking the inverse discrete sine transform back to real space, giving $\psi(x,y,z_{k+1/2})$ (see Eq 3.1 and 3.2). This integration in phase space is exact. Then, $\psi(x,y,z_{k+1/2})$ is used as initial data $\psi(x,y,z_k) = \psi^*(x,y,z_{k+1/2})$ in integrating the remaining terms over the full time step from (x,y,z_k) to (x,y,z_{k+1}) (see Eq 3.3 and 3.4). Finally, $\psi(x,y,z_{k+1})$ is then used as the initial data $\psi(x,y,z_{k+1/2}) = \psi(x,y,z_{k+1})$ for integrating the transversal term the final half time step exactly using the same procedure as in the first step (see Eq 3.5 and 3.6).

首先，初始值是$\psi(x,y,z_0) = f(x,y)$。使用离散正弦变换（DST)所以可确切地在相空间的半个时间步从(x,y,z_k)到$(x,y,z_{k+1/2})$积分横向项ψ^*，然后使用离散正弦逆变换变成到实空间，条件是$\psi(x,y,z_{k+1/2})$ (方程 3.1 和 3.2)。第 2，被用作$\psi(x,y,z_k) = \psi^*(x,y,z_{k+1/2})$的初始值。来积分剩下的的在实空间$(x,y,z_k)$到$(x,y,z_{k+1})$ 的项(方程 3.3 和 3.4)。最后，$\psi(x,y,z_{k+1})$被当作初始值，用第 1 步进的方法：用离散正弦变换，变$\psi(x,y,z_{k+1})$到相空间ψ^{**}，再确切地积分横向项$(x,y,z_{k+1/2})$to (x,y,z_{k+1}) (方程 3.5 和 3.6)。最后，和第一步的步骤一样，$\psi(x,y,z_{k+1})$以初始值$\psi(x,y,z_{k+1/2}) = \psi(x,y,z_{k+1})$用于最后的半个时间步长。

$$\psi^*(x,y,z_{k+1/2}) = \int_{z_k}^{z_{k+1/2}} i\delta_z \psi \, dz = \int_{z_k}^{z_{k+1/2}} -\nabla_\perp^2 \psi \, dz \tag{3.1}$$

$$\psi^*(x,y,z_{k+1/2}) = IDST\left(e^{-\frac{ik}{2}((\frac{x\pi}{b-a})^2+(\frac{y\pi}{b-a}^2))} \times DST(\psi(x,y,z_k))\right) \tag{3.2}$$

$$i\partial_z \psi + \alpha\psi^2\psi - \varepsilon\psi^4\psi - \gamma\psi^{2K}\psi + i\nu\psi^{2K-2}\psi = 0 \tag{3.3}$$

$$\psi(x,\hat{y},z_{k+1}) = \int_{z_k}^{z_{k+1}} \partial_z \psi \, dz = \int_{z_k}^{z_{k+1}} +i\alpha\psi^2\psi - i\varepsilon\psi^4\psi - i\gamma\psi^{2K}\psi - \nu\psi^{2K-2}\psi \, dz \tag{3.4}$$

$$\psi^{**}(x,y,z_{k+1}) = \int_{z_{k+1/2}}^{z_{k+1}} i\partial_z \psi \, dz = \int_{z_k}^{z_{k+1/2}} -\nabla_\perp^2 \psi \, dz \tag{3.5}$$

$$\psi^{**}(x,y,z_{k+1}) = IDST\left(e^{-\frac{ik}{2}((\frac{x\pi}{b-a})^2+(\frac{y\pi}{b-a}^2))} \times DST(\hat{\psi})\right) \tag{3.6}$$

4 NUMERICAL RESULTS AND DISCUSSION 结果和讨论

4.1 Gaussian Beams 高斯光束

4.1.1 Simple Gaussians and Symmetry 简单高斯和对称

The results came close to matching expectations. Exponential convergence in mesh size was expected and observed as shown in the quintic nonlinearity only case shown below. Closer investigation found that such very fast convergence only occurred with mesh size (h) below $h = 1/4$. Convergence of only first order was observed for the time step (dt). Quadratic convergence was expected.

结果与对应预期十分接近。下方展示的五阶非线性情况，结果显示网格大小如预期呈现指数收敛。。进一步检查发现这种快速指数收敛只发生在 h < ¼的情况下。 结果显示随时间步距的一阶收敛，而不是预期的二阶收敛。

Table 1. Convergence order under different parameters at t=0.4

For initial data: $\psi(x,y,0) = \frac{2^{1/4}}{2\varepsilon} exp(-(x^2+2y^2))$

Time Step:	Dt=0.001	Dt=5.0e-4	Dt=2.5e-4 Dt=1.25e-4	Dt=6.25e-5	
Error (L2 norm)	5.06e-03	2.49e-03	1.21e-03	5.71e-04	2.53e-04
$\lvert e(n+1)\rvert / \lvert e(n)\rvert$	4.93e-01	4.86e-01	4.71e-01	4.42e-01	

Mesh Size:	h=1	h=1/2	h=1/4	h= 1/8	h= 1/16
Error (L2 norm)	1.5446	0.4106	7.28e-02	1.77e-04	1.15e-10
$\|e(n+1)\|/\|e(n)\|$	0.2658	0.1772	2.43e-03	6.51e-07	

Table 1. Convergence order under different parameters at t=0.4

For initial data: $\psi(x,y,0) = \frac{2^{1/4}}{2\varepsilon} exp(-(x^2+2y^2))$

Time Step:	Dt=0.001	Dt=5.0e-4	Dt=2.5e-4	Dt=1.25e-4	Dt=6.25e-5	
Error (L2 norm)	5.06e-03	2.49e-03	1.21e-03		5.71e-04	2.53e-04
$\|e(n+1)\|/\|e(n)\|$	4.93e-01	4.86e-01	4.71e-01		4.42e-01	

Mesh Size:	h=1	h=1/2	h=1/4	h= 1/8	h= 1/16
Error (L2 norm)	1.5446	0.4106	7.28e-02	1.77e-04	1.15e-10
$\|e(n+1)\|/\|e(n)\|$	0.2658	0.1772	2.43e-03	6.51e-07	

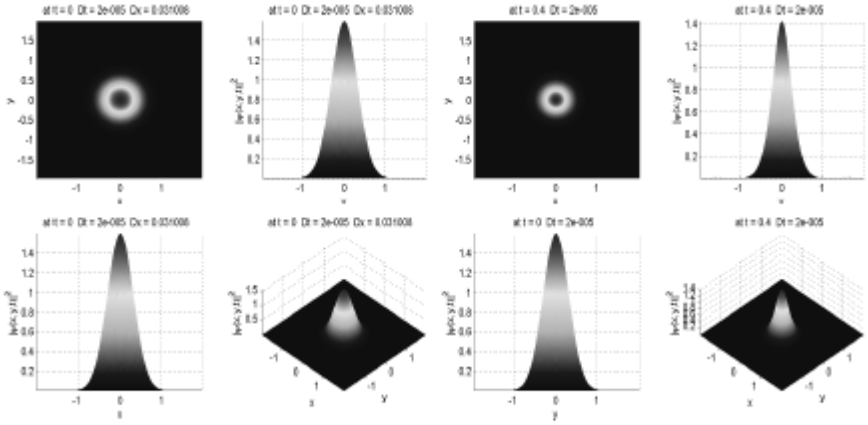

Figure 1: $|\psi|^2$ with initial radial symmetry, Dt=0.00002, 5, with only quintic damping, K=3 (a) t=0, (b) t=0.4.

图 1: $|\psi|^2$初始径向对称, Dt=0.00002, 5阶阻尼 K=3 (a) t=0, (b) t=0.4.

As can be observed from the figure above (Fig. 1), the quintic nonlinearity had a narrowing or focusing effect in the given timeframe. Initially the central density of the beam increases, then comes to its maximum, and from there on decreases, converging to zero, and diffusing in an oscillatory manner.

如上图（图 1）所示，在使用的时间范围，五阶非线性对结果具有变窄和聚焦效应。起初，光束中部的密度增长，直到达到 最大值后开始减小，相对于 0 收敛，同时摆动状地扩散。

They compare the effects of the domain size, number of grid points, (and in combined

effect mesh size), and time step size near what appears to be the radius of convergence. For the following tests, the cubic nonlinear case was used unless otherwise noted. In holding all else constant, one can observe the effect the stepsize has on the laser. Around this cusp, the smaller stepsize yields better results. It is thinner, meaning it dissipates slower. It is also more stable. This can be seen by the oscillations on the top of the profile.

它们比较了类似收敛半径附近的取值范围、网格点数量(和网距)和时间步距的影响. 如果没有另外说明，以下试验皆使用三阶非线性情况。如果只改变时间步距长度，保持别的变量恒定，可以观察到时间长度对激光的影响。在第一类尖点的附近，时间步距越短结果越好。步距越短，结果越细，或者说驱散得比较慢；而且步距越短，结果越稳定。这些可从侧视图上方的振荡观察到。

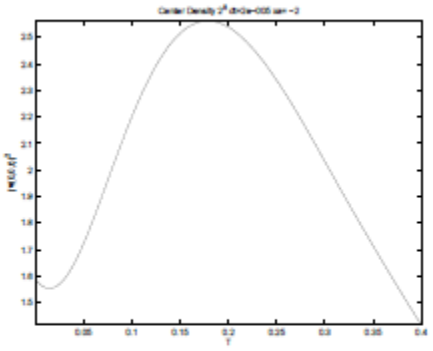

Figure 2: $|\psi(0,0,t)|^2$ Center density with initial radial symmetry, Dt=0.00002, with only a quintic daming, K=3 (a) t=0, (b) t=0.4.

图 2: $|\psi(0,0,t)|^2$ 中密度，初径向对称, Dt=0.00002, 5阶阻尼K=3 (a) t=0, (b) t=0.4.

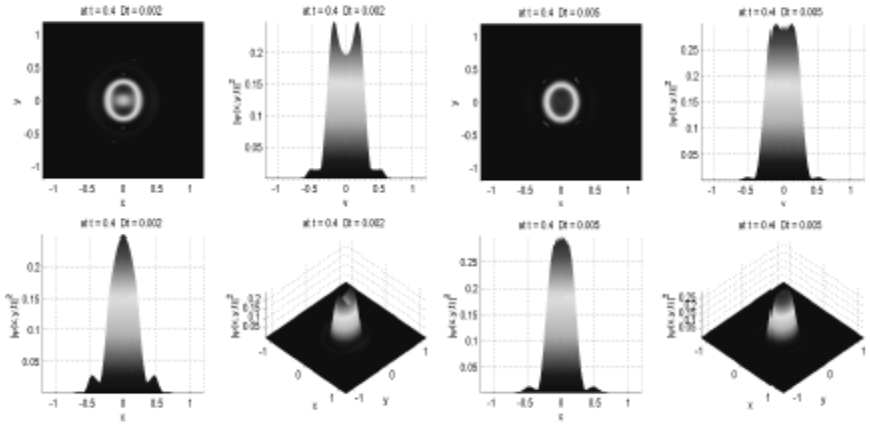

Figure 3: Gaussian with cubic nonlinearity and elliptical symmetry with (a) $Dt = .002$ and (b) $Dt = .005$.

Figure 3: Gaussian with cubic nonlinearity and elliptical symmetry with (a) $Dt = .002$ and (b) $Dt = .005$.

图 3: 3阶非线性高斯函数和椭圆性对称(a) $Dt = .002$ 和 (b) $Dt = .005$.

To ensure that the results are stable with respect to the number of data points, for time step size (Dt) held constant, results with $2^9 \text{x} 2^9$ and $2^8 \text{x} 2^8$ grids are displayed in Figure 4. As there is no visible difference, it can be said that the $2^8 \text{x} 2^8$ grid is sufficient for this level of analysis and is not a source of error.

为了保证结果相对于数据点数量的 稳定性，保持时间长度(Dt)不变 $2^9 \text{x} 2^9$ 和 $2^8 \text{x} 2^8$ ç网的结果在图 4 显示。因为没有可见的不同，所以说 $2^8 \text{x} 2^8$ 网已经足够作这样的分析，不会导致分析错误。

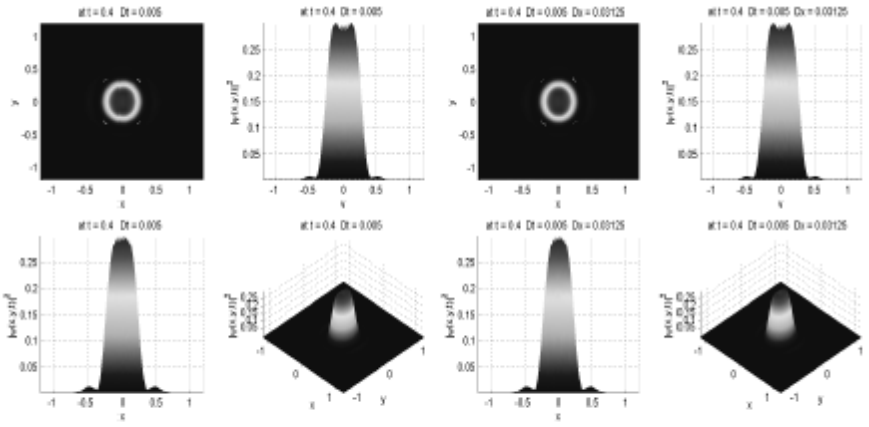

Figure 4: Comparing mesh sizes for Gaussian with initial elliptical symmetry and cubic damping with (a) $h = 8/2^9 = 1/64$, (b) $h = 8/2^8 = 1/32$.

图 4: 比较网络尺寸关于初始椭圆性对称的高斯函数有3阶阻尼 (a) $h = 8/2^9 = 1/64$, (b) $h = 8/2^8 = 1/32$.

Since the marginal number of grid points does not have a large effect at this level, it can be inferred that the instability pattern is the result of time step and the chosen domain size, in other words, choosing the appropriate window so the assumption that the border values are zero is practically valid. How many grid points or how dense the mesh is is not the determining factor at this point.

因为边缘网络点额在这个水平的影响不大，可以推测非稳定性跟时间步长度和定义域范围有关系。或者说，选择合适窗口[范围]让边界数等于 0 的假定成立是有效的。[此时，]网络点数量和网络密度的影响[不是决定条件]。

Time step size, though, does have a visible effect on the propagating beam. This is clearly seen in the center densities ($|\psi(0,0,t)|^2$). With a smaller step size, the larger the maximum center density. This implies that the time step used is not short enough to ensure accurate results, and will only be used to give a general sense the beam and other variables' relative effects.

时间步差大小对传播的光束有可观察到的影响。这在中点密度 ($|\psi(0,0,t)|^2$)表现得很清楚。时间差越小，最大中点密度越大。这意味着使用的时间步距过长，不足以确保精确的结果；只能用来大致表现光束和其他变量的相对影响。

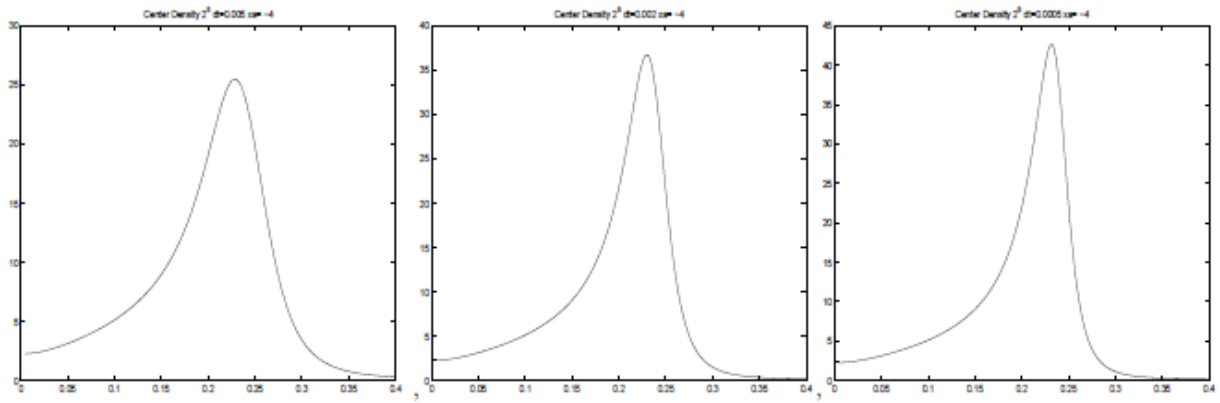

Figure 5: Center densities $|\psi(0,0,t)|^2$ with elliptical symmetry, cubic damping, 2^8 mesh,' $K = 2$, $(x,$

Figure 5: Center densities $|\psi(0,0,t)|^2$ with elliptical symmetry, cubic damping, 2^8 mesh, ' $K = 2$, $(x, y) = [-4,4]$, $h = 1/32$, (a) $Dt = .005s$, (b) $Dt = .002s$, (c) $Dt = .001s$.

图 5: $|\psi(0,0,t)|^2$ 初始情况椭圆性的对称中心密度，3阶阻尼, 2^8 网络, ' $K = 2$, $(x, y) = [-4,4]$, $h = 1/32$, (a) $Dt = .005s$, (b) $Dt = .002s$, (c) $Dt = .001s$.

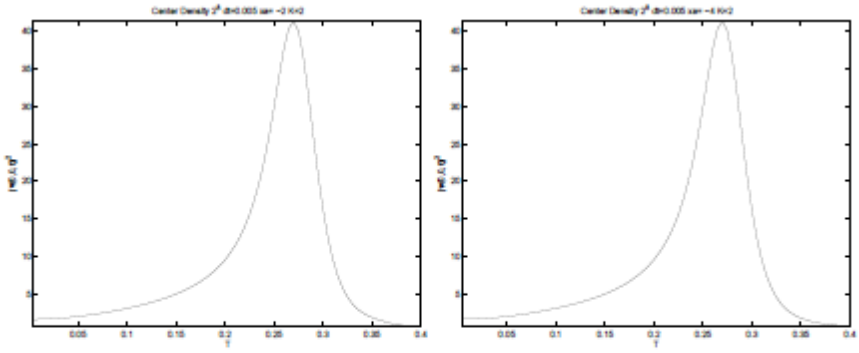

Figure 6: Center densities $|\psi(0,0,t)|^2$ with elliptical symmetry, cubic damping, 2^8 mesh, $Dt = .005s$, $K = 2$, (a) $[-2,2]^2$, $h = 1/64$, (b) $[-4,4]^2$, $h = 1/32$

图 6: $|\psi(0,0,t)|^2$ 初始情况椭圆性的对称中心密度，3阶阻尼, 2^8 网络, $Dt = .005s$, $K = 2$, (a) $[-2,2]^2$, $h = 1/64$, (b) $[-4,4]^2$, $h = 1/32$

The above figures (Figure 6a,b) compare center densities for the two previous different domains, $(x, y) \in [-2,2]$ and $(x, y) \in [-4,4]$. Both have the same number of grid points, so Dx is twice as fine in the $[-2,2]$ case. It can be observed that while this had an effect on instabilities in the overall function, it did not have a significant effect on the center density value.

上图（图 6a,b）比较之前的两个不同范围的中点密度，$(x,y)\in[-2,2]$ and $(x,y)\in[-4,4]$.它们两的网络点一样多，所以 Dx 比[2,2]情况精细度的两倍。可以观察到这对函数的非稳定有影响；然而对中点密度影响不大。

In most physical sources, K=8 is the minimum number of photons for ionization, [2] so we will compare the results and effectiveness of the algorithm for K=8 and K=2. Below compares the center density plots for each.

在真实物理媒介，K=8是最小让电离的光子数量[2]，所以我们首先比较K=2和K=8算法的结果和有效性。下方比较它们的中点密度图。

As can be observed, the higher K value resulted in a beam's density ($|\psi|^2$) getting wider and shorter (not having as large a maximum density). The instability is most pronounced on the peak/plateau of the $K=8$ graphs and not for $K=2$ stems from the boundaries - as the $K=8$ case dissipates faster, it reaches the boundaries faster which conflicts with the assumption that the boundary values are zero. The peak in the $K=8$ case is also almost flat, while the $K=2$ Gaussian is a much sharper curve. With sufficiently wide boundaries ([-4,4]x[-4,4]), the propagations are smoother and better behaved. The center density patterns for $K=2$ and $K=8$ follow the same general pattern of increasing density/focusing to a maximum and then dissipating, though in the $K=2$ case, the maximum density is much greater and is reached much later than in the $K=8$ case and dissipates much more quickly.

如结果所示，K越大，光束密度$|\psi|^2$越宽也越短（没有那么高的最大密度）。这种不稳定性在$K=8$的图中的峰会/平表现得最明显，在$K=2$的边界却表现得不明显。这是因为$K=8$，它也较快达到边界。这与边界值为0的假设相矛盾。$K=8$的情况中的峰值接近于水平段，而$K=2$的情况中高斯曲线更为尖锐。如果使用足够宽的边界（$[-4,4]x[-4,4]$)），散播就会更加平滑良好。$K=2$和$K=8$的中点密度均在达到最大值前增加，然后分散。可K=2时最大密度比K=8时的最大密度大的多，而且到达最大值也比$K=8$时慢的多然后驱散得快得多.

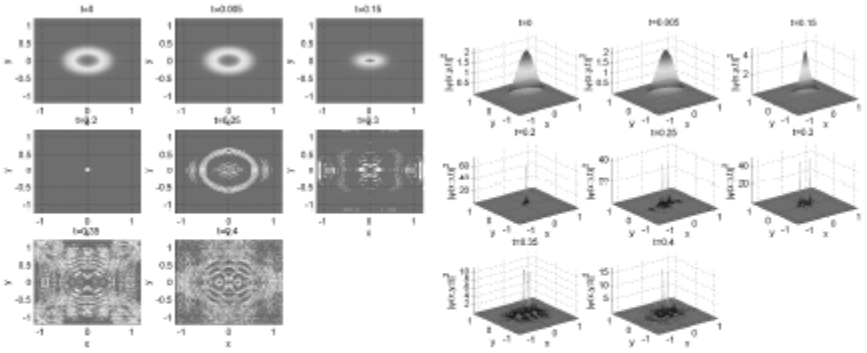

Figure 7: $|\psi(0,0,t)|^2$ with elliptical symmetry, cubic damping, 2^8 mesh, $Dt = .005s$, $K = 2$, $[-4,4]^2$, $h = 1/32$, (a) overhead view (b) 3D view

图 7: $|\psi(0,0,t)|^2$ 初始有椭圆性的对称,3阶阻尼, 2^8 网络, $Dt = .005s$, $K = 2$, $[-4,4]^2$, $h = 1/32$, (a) 顶视图 (b) 3维视图

An interesting case is when the beam is taken at very close view: $(x, y) = [-4,4] * \omega_0$, $\omega_0 = 0.3$. (ω_0 is a physical value indicating the initial beam width used by Vincotte-Berge. In modeling their physical situations, $(x, y) = [-4,4] * \omega_0$ is a part of nondimensionalization. Here, it should have only had a scaling effect. Calculation contradicted this idea.) The same initial beam used above (same parameters) yields vastly different results. The beam progression/propagation is as follows (see figure 7): First it self-focuses to a very high magnitude, much higher than in the previous cases (a single Gaussian dominates the profile) (t=0.2s). Then it relaxes back down, defocusing, and then gives rise to two filaments spaced along the major axis of the initial beam (the original elliptical shape when viewed from overhead is still recognizable at this point, t=0.25s.) Then these two filaments give rise to two more, one the same axis, a little farther from the center (as the original two filaments go down, the new two rise). Then, after these new two reach their maximum and relax, two new filaments grow, on opposite ends of the minor elliptical axis. It should be noted that none of these filament pairs ever reach a magnitude similar to the first filament. It then goes through this cycle of one axis growing two filaments, them relaxing and giving rise to two smaller filaments on the perpendicular axis, until the beam has decomposed to chaos and dissipation. This does not happen when the domain is changed from [-4,4] to [-1.2,1.2] or [-8,8] to [-2.4,2.4].

ω_0是一个物力数值，用它来表示最初光束宽度。在建立其物理模型时，$(x, y) = [-4,4] \times \omega_0$是无量纲化的部分。这里，应该仅有比例效应。计算与这个想法矛盾。）跟上面一样的初始光束（参数相同）得到的结果很不一样。光束是这样传播的（看图 7）：首先光束自己聚焦到很高的强度，比之前的情况高很多（一个高斯决定了其侧视图）（$t = 0.2$）。然后，光束松散下来，散焦，然后两个丝状体出现在初始光束的轴两边（俯视图还可以看到原来的椭圆形，$t = 0.25s$ 然后沿着同一轴，这两个丝状体外侧出现另两条

丝状体（共四条）（随着原有的两条丝状体变淡，丝状体显现）。这两条新的丝状体的增长到他们的最大强度后散淡，然后另两个新丝状体在椭圆短轴的两端出现。值得注意的是后出现的两对丝状体的最大强度都不不会超过初始的第一对丝状体。这个周期会一直继续：一对丝状体沿着椭圆的一轴增强，达到最大值后散淡，然后在垂直的另一条轴两边出现一对新的丝状体。这个周期发生很多次后，光束逐渐变淡、分散。在定义域在[–4,4]到[–1.2,1.2]或[–8,8]到[–2.4,2.4]时，无以上现象发生。

For the non-radial symmetry (elliptical initial beam), the figures below (Fig. 8a and b) demonstrate, with a wider domain, the smaller time step led to a much larger center density when K=2, but had a much more subtle effect when K=8 (where the larger time step led to only a marginally higher center density). All cases had no instability issues due to the sufficiently large domain ($(x, y) \in [-4,4]$). From an elliptical (without radial symmetry) initial condition, the beam quickly approached a more circular distribution, as seen in the contour plot below. The beam does converge towards radial symmetry, but in an oscillatory manner. After starting with elliptical distribution with the x axis as the major axis of symmetry, it approaches radial symmetry, continues to an elliptical pattern with the y axis as the major axis, and visa versa. ($Dt = .005$, $K = 8$ was used as the representative case).

对于非径向堆成（初始光束是椭圆性的），下图（图 8a,b）说明，在较大范围情况下，当 K=2 时，逐渐减少时间间隔会导致形成较大的中心密度比较小时间步差的情况，如果 K=2 让比较大的中密度，但是，当 K=8 时，时间步长效应会更不明显。可是让 K=8，这个效应比较微妙的（较大的时间步长会导致中心密度变化的比较小有比较大的时间步差就让中密度比较大一点）。由于范围足够大，所有的情况都不会有不稳定的问题全部的情况没有非稳定的问题因为范围大足够了($(x, y) \in [-4, 4]$)。如果初始情况是椭圆性（没有径向对称），光束就会如下图所示（图 11）快速趋向于径向分布光束很快地靠近比较圆性形。请看下的图（图 11）。当光束在以 x 轴为主要对称轴的方向上椭圆分布时，其趋向于径向对称，而当 y 轴作为主轴时，光束依然为椭圆型。光束摆动地收敛到径向对称。开始有椭圆性分布，x 轴是长轴的对称轴以后，它靠近径向对称，继续到 y 周是长轴，然后等等。（Dt = .005, K=8 使用典型的情况）。

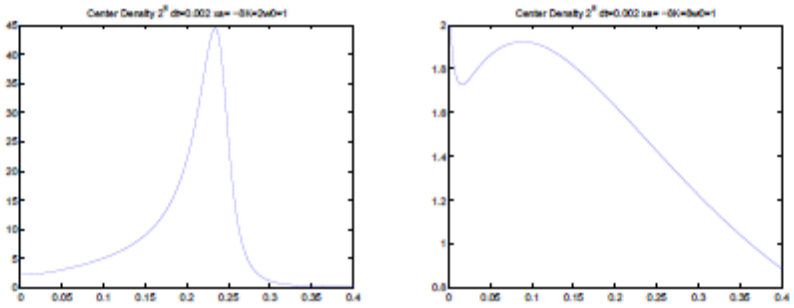

Figure 8: $|\psi(0,0,t)|^2$ Center density of an initially elliptical Gaussian with cubic damping, ' 2^8 mesh, $Dt = .002s$, $(x,y) = [-4,4]$, $h = 1/32$, (a) $K = 2$ (b) $K = 8$

图 8: $|\psi(0,0,t)|^2$ 初始椭圆性高斯的中密度，3阶阻尼 ' 2^8 网络, $Dt = .002s$, $(x,y) = [-4,4]$, $h = 1/32$, (a) $K = 2$ (b) $K = 8$

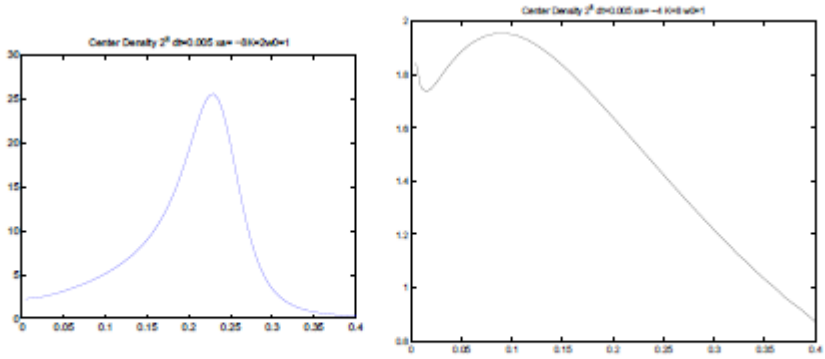

Figure 9: $|\psi(0,0,t)|^2$ Center density of an initially elliptical Gaussian with quintic damping, 2^8 mesh, $Dt = .005s$, $(x,y) = [-4,4]^2$, $h = 1/32$, (a) $K = 2$ (b) $K = 8$

图 9: $|\psi(0,0,t)|^2$ 初始椭圆性高斯的密度，5阶阻尼 2^8 网络, $Dt = .005s$, $(x,y) = [-4,4]^2$, $h = 1/32$, (a) $K = 2$ (b) $K = 8$

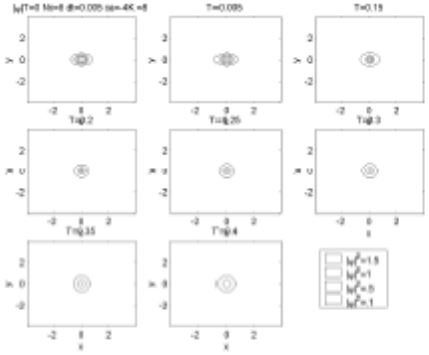

Figure 10: $|\psi|^2$ Contour plot of an initially elliptical Gaussian with quintic damping, 2^8 mesh, $Dt = .005s$, $(x, y) = [-4,4]^2$, $h = 1/32$, $K = 8$

图10: $|\psi|^2$ 等高线图：初始椭圆性高斯，5阶阻尼 2^8 网络, $Dt = .005s$, $(x, y) = [-4,4]^2$, $h = 1/32$, $K = 8$

When the x and y dimensions were multiplied by $\omega_0 = .3$ ($(x, y) = [-4,4] * \omega_0$), there is an interesting difference when $K = 2$ between the $dt = .002$ and $dt = .005$ cases. For the smaller time step, there was a slightly different pattern of development. It was almost exactly the same phases as described previously, but there was the development of a second strong center spike in density. This did not occur in the larger time step, which resembled the special pattern described previously. For $K = 8$, just as in the normal case, results were very similar for both time steps, with the larger time step having a slightly greater central density.

x和y范围(当x和y)乘以ω0 = .3 ((x, y) = [−4, 4] ∗ ω0)，K=2时，Dt=0.002的情况跟Dt=0.005的有有意思的不同我们采用不同的Dt值（Dt=0.002，0.005），发现这两种情况存在有趣的不同。当Dt=0.002时，发展方式 有小小的不同,它的步骤跟我们已经的前面描述基本相同，只是在此时出现了第二个大的中心密度峰形。这种现象在时间步差比较大时不发生，因为大的时间步差代表之前已经描述过的特别方式。K=8时,跟平均的情况一样，在两个时间步差下的结果差不多，唯一不同的是比较大的时间步差的中心密度比较大一点.

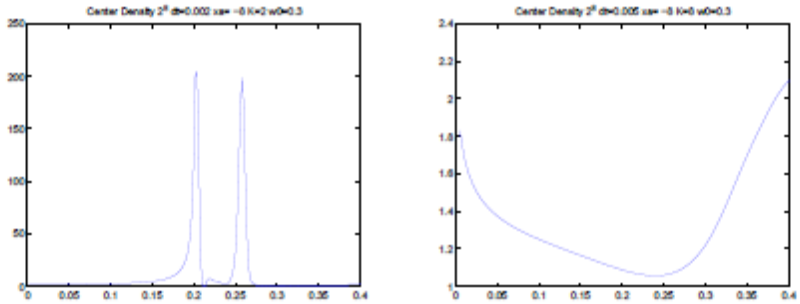

Figure 11: $|\psi(0,0,t)|^2$ Center density of a Gaussian with radial symmetry and quintic damping, 2^8 mesh, $Dt = .002s$, $(x,y) = [-4,4]^2$, $h = 1/32$, $\omega_0 = .3$, (a) $K = 2$ (b) $K = 8$

图 11: $|\psi(0,0,t)|^2$ 径向的对称的高斯的中心密度，5阶阻尼, 2^8 网络, $Dt = .002s$, $(x,y) = [-4,4]^2$, $h = 1/32$, $\omega_0 = .3$, (a) $K = 2$ (b) $K = 8$

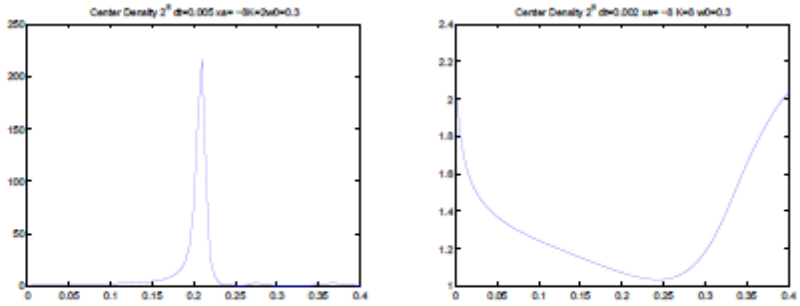

Figure 12: $|\psi(0,0,t)|^2$ Center density of a Gaussian with cubic nonlinearity, 2^8 mesh, $Dt = .005s$, $[-4,4]^2$, $h = 1/32$, $\omega_0 = .3$, (a) $K = 2$ (b) $K = 8$

图 12: $|\psi(0,0,t)|^2$ 径向对称高斯的中心密度，3阶阻尼[非线性] 2^8 网络, $Dt = .005s$, $[-4,4]^2$, $h = 1/32$, $\omega_0 = .3$, (a) $K = 2$ (b) $K = 8$

Similar behavior was observed in the analogous radial symmetry case for both $K = 2$ and $K = 8$, though in the $K = 2$ case there was no oscillating axial filament pairs. Instead, after the dominating central spike collapsed, a ring rose up and went on to follow an oscillating cycle. The $K = 8$ case was well behaved, very similar to the nonradial symmetry case.

在类似径向对称情况，K=2和K=8的性质很相似，可是在K=2时，不存在摆动的轴双

丝状。相反，当原来的最大的峰形消失时，一个环形出现并且在之后的摆动周期中持续存在。K=8的情况比较好，跟非径向对称情况的很相似。

$$\psi(x,y,t)=\frac{2^{1/4}}{\sqrt{\pi\varepsilon}}exp(-\frac{x^2+\gamma_y y^2}{2\varepsilon}) \tag{4.1}$$

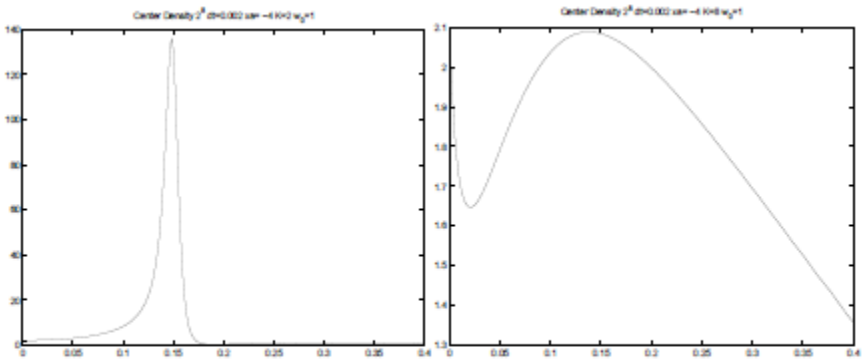

Figure 13: $|\psi(0,0,t)|^2$ Center density of a Gaussian with radial symmetry and cubic nonlinearity, 2^8 mesh, $Dt=.002s$, $[-4,4]^2$, $h=1/32$, $\omega_0=1$, (a) $K=2$ (b) $K=8$

图 13: $|\psi(0,0,t)|^2$ 径向对称3阶非线性的高斯的中心密度 2^8 网络, $Dt=.002s$, $[-4,4]^2$, $h=1/32$, $\omega_0=1$, (a) $K=2$ (b) $K=8$

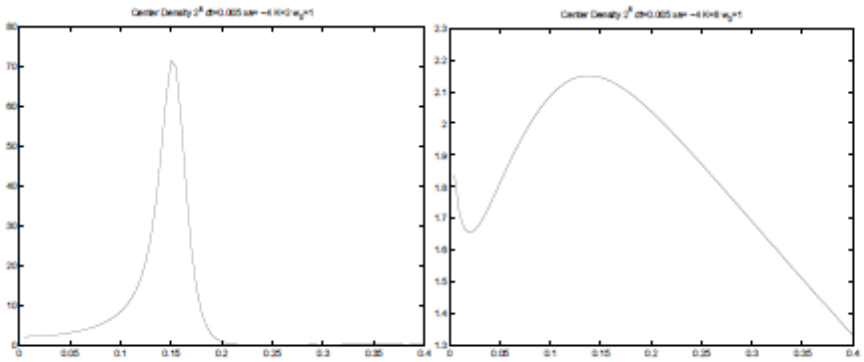

Figure 14: $|\psi(0,0,t)|^2$ Center density of a Gaussian with radial symmetry, cubic and quintic damping, 2^8 mesh,' $Dt = .005s$, $(x,y) = [-4,4]$, $h = 1/32$, $\omega_0 = 1$, (a) $K = 2$ (b) $K = 8$

图 14: $|\psi(0,0,t)|^2$ 径向对称3阶和5阶非线性的高斯的中心密度, 2^8 网络,

' $Dt = .005s$, $(x,y) = [-4,4]$, $h = 1/32$, $\omega_0 = 1$, (a) $K = 2$ (b) $K = 8$

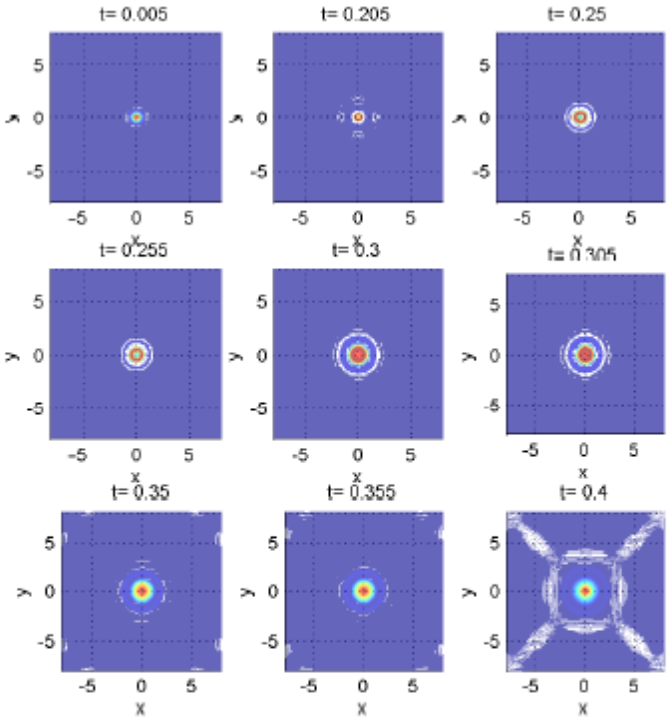

Figure 15: $|\psi|^2$ Propagation of a Gaussian with radial symmetry, 2^8 mesh, $Dt = .005s$, $(x, y) = [â\square 4,4]$, $h = 1/32$, $\omega_0 = 1$, $K = 2$

图 15: $|\psi|^2$ 径向对称高斯传播, 2^8 网络, $Dt = .005s$, $(x, y) = [â\square 4,4]$, $h = 1/32$, $\omega_0 = 1$, $K = 2$

When both the cubic and quintic nonlinearities are combined and the beam is not radially symmetric but elliptical, and $K = 5$ $\delta_2 = .02$, $\delta_3 = .01$, where δ_2 is the coefficient of the cubic nonlinearity and δ_3 is the quintic coefficient, the overall effect is the significant narrowing along the minor axis. When the cubic and quintic terms are both used and $K = 3$, the pattern involving a massively dominating center Gaussian, but seems to be retarded slightly. In other words, the sequence of growth and decay does not start until later.

当3阶和5阶非线性联合时，初始光束对称是椭圆的，不是径向的，K=5，δ2=0.02，δ3=.01，δ2是3阶非线性的系数，δ3是5阶非线性的系数，整体效应是在短轴上明显地变窄。当3阶和5阶项都被使用，同时K=3时，在传播中存在一个支配的高斯中心，只是比较慢一点。换句话说，增长和降低的序列比较晚开始。

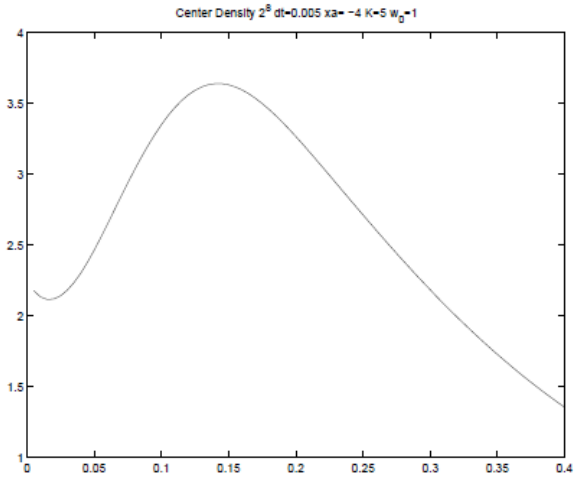

Figure 16: $|\psi(0,0,t)|^2$ with radial symmetry, 2^8 mesh, $Dt = .005s$, $[-4,4]^2$, $h = 1/32$, $\omega_0 = 1$, $K = 5$

图 16: $|\psi(0,0,t)|^2$ 径向对称 2^8 网络, $Dt = .005s$, $[-4,4]^2$, $h = 1/32$, $\omega_0 = 1$, $K = 5$

4.1.2 Flat-topped Gaussians 有平滑顶部的高斯

In modeling more complex beams, such as the propagation of a flat-top Gaussian beam with steep sides, the results are quite pleasing, bearing strong resemblance to the exact information (Figure 1). Varying the mesh size and time step size did produced similarly shaped results. The main difference being how fast the filaments grow, not where in the x,y plane they grow. The trend was the smaller the mesh size, the higher the filament's energy density/fluence. Time step size converged in $Dt = [.02,.04]$, so the fluence pattern error for time steps smaller than .02 does not change very much. With $Dt > .02$, the filament magnitude increases very quickly as Dt increases. Thus, it is more efficient to spend computation time on a finer mesh than a smaller time step as long as the $Dt < .02$.

在模拟比较复杂的光束时，比如有平滑顶部和陡坡面的高斯波，我们的结果是很好的，跟试验的精确结果非常相似（图 1）。改变网距和时间步差，我们得到形状相似的结果。最主要的不同是丝状增大的速度，而不是它们的位置。在这里，普遍的趋势是网距越短，丝状能量密度/能量流量越高。时间步差在 $Dt = [.02,.04]$ 时是收敛的，所以能量流量的误差在使用比 $Dt = 0.02$ 短的时间步差时变化不大。当 $Dt > 0.02$ 时，丝状数量随着 Dt 的增长，增长得很快。[Dt 越大，丝状很快地提高]。因此，当 $Dt < 0.2$ 时，用比较细的网距比用比较短的时间步差计算更有效率。

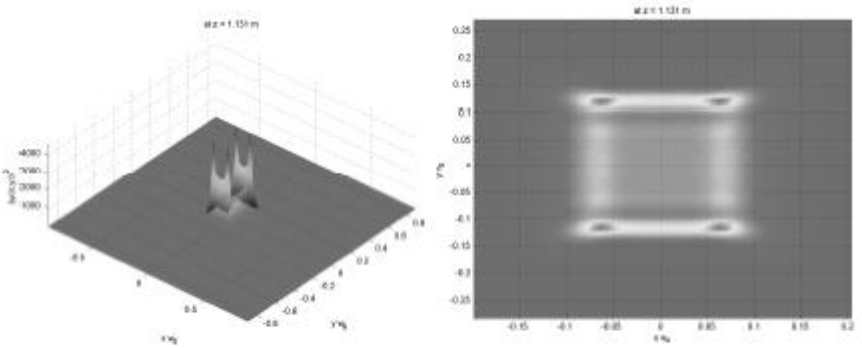

Figure 17: Flat-top pulse profile and contour plot.
图 17: 有平滑顶部和陡坡面的高斯波.

4.2 Ring Beams 轮胎性光束

4.2.1 Doughnut beams (without vortexing) 轮胎性光束(非涡性)

$$E(z=0) = A_{in}(r/\omega_0)e^{-r^2/\omega^2+i\theta} \quad (3)$$

Doughnut beams proved to be more sensitive to time step size, especially in terms of radius of convergence. Compare the two images below. For Dt=.2 m, and in Fig. 2, dt=2.0 m. Typically the beam reduces to a ring of filaments which seem to be vortexing. This pattern of vortexing holds for a long time. As can be seen in Figure 18, for certain conditions the beam splits, converges rapidly, and then "explodes," leaving four tightly vortexing filaments.

轮胎形光束对时间步差比较敏感，尤其是它们的收敛半径。比较下面的图片（图 18,19）。在图 18 中 $Dt = 0.2m$，在图 22 中 $Dt = 2.0m$。一般情况下，这些光束成了好像涡流的轮胎性丝状。这样的涡流形态会持续传播好久。从上面的图片（图 16)可以看到，在某些情况下光束会分开，更快地收敛，然后爆炸，最终只剩下四个紧紧地涡流的丝状。

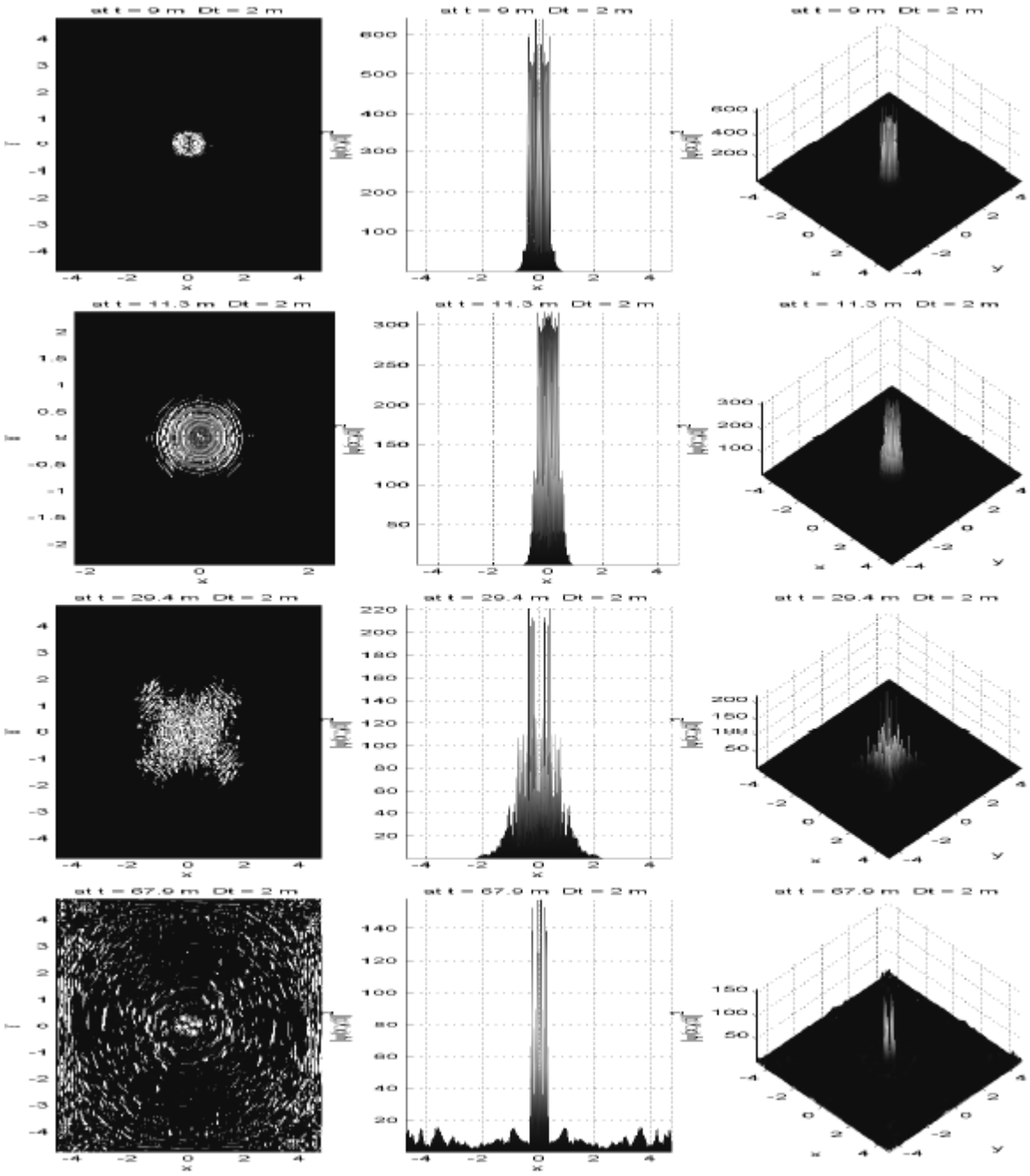

Figure 18: Doughnut pulse profile $|\psi|^2$, during atypical propagation。

图 18: 轮胎性脉搏侧面$|\psi|^2$, 不典型的传播。

4.2.2 Vortexing beams 涡性光束

$$E(z=0) = A_{m,1}(r/\omega_0)^{|m|} e^{-r^2/(2\bar{r}_{m,1}^2)+im\theta} \quad (2)$$

Given the right initial conditions, a beam (ring shaped) will vortex. This makes it more robust and stable than its nonvortexing counterpart, the doughnut, as previously described. Thus, it will continue to propagate in an orderly pattern rather than dissipate to chaos. As the beams propagate, they generally become thinner and thinner until they become filaments of very high energy intensity. These filaments are very robust, able continue in this state on the hundreds of meters scale. After which, they inevitably begin to dissipate in a seemingly chaotic manner. When the beams are of opposite spin, the initial pattern looks like two lop-sided arcs.

在合适的初始情况下，一个环形光束会形成涡流。这让它比非涡流的的稳定的多。因此，形成涡流的会继续有秩序的传播而不驱散到混乱。光束传播的时候，一般情况下，它们会越来越细，直到形成了高能的丝状。这些丝状很稳定，可这样地继续传播几百米。几百米后，它们不可避免地开始以看起来混乱的状态驱散。如果这两个光束以反方向旋转，它们的初始形态看起来像两个不平衡的弧线。

4.3 Multiple Beams多重光束

4.3.1 Multiple Gaussians 多重高斯光束

After the effectiveness of the model had been established, it was extended to study the ways beams interact with each other, not just with themselves and with atmosphere.

在研究了这个模型的有效性之后，我们继续研究了这个算法模型中光束之间的相互影响，而不是仅仅研究它们与自己和大气的关系。

In the first example, two beams with cubic and quintic nonlinearities are set next to each other, with identical initial data. The initial data of each beam is a Gaussian without radial symmetry (pulled in the x direction). The centers of each beam are initially separated by 2 meters, in case 1 in the x direction, and in the y direction in case 2. In both cases, the results were very similar. As the two beams propagated and dissipated, a third peak formed in center of the two initial beams. Eventually, this peak dominates the profile. The center density plots show when the center peak begins to dominate. All cases have similar profiles with very little variation in critical points. The center peak begins to dominate at $t = .25s$, and then grows rapidly. At about $t = .65s$, it too begins to decay and dissipate. It appears to be becoming periodic after $t = 1s$. This is feedback from when the the dissipation reached the boundaries, making them not equal to zero and adding error to the calculations.

试验一：两个有3阶和5阶非线性光束初始情况下被并排放置。，参数相同，初始情况相同，初始情况是非径向对称（x轴跟它们的长轴平行）的高斯。两个光束的中心的初始距离是2米，在第一种情况下它们沿x方向分开，在第二种情况下它们沿y方向分开。

两个情况下的结果很相似。在两个光束传播和发散过程中，在它们的中点出现了第三个峰形。最后，这个峰形主宰了整个波形。中心密度图演示了在什么时候中心峰形主宰了整个波形。所有情况下的波形都很相似，临界点的变化很小。中心峰在$t = 0.25s$时主宰整个波形，然后继续快速增大。在$t = 0.65s$左右，波形开始减退发散。t=1.0s后，波形开始呈现周期性。这个误差的原因是光束发散到边界，所以边界数量不等于0。

It was interesting that when aligning two elliptical initial Gaussian beams along their major axis, with their centers both 1m from the origin, ended up producing a Gaussian with contours that were elliptical with the opposite axis as the major axis. Thus, while the x axis was the major axis initially, the y axis was the major axis in the end. When the beams are aligned along their minor axis, the resultant beam is ultimately (by $z = 1.5m$) dominated by an elliptical Gaussian with its major axis perpendicular to the axis connecting the centers of the two initial beams. Thus, the orientation of the individual beams is not the determining factor in the orientation of the resultant beam, but the axis connecting the two centers.

有趣的是， 当两个初始椭圆性的光束沿着长轴排列，中心距离原点1m时，它们最终形成一个有着椭圆形等高线的高斯，这个椭圆型的对面的轴成了长轴。因此，虽然原来x轴是长轴，最终，y轴成为长轴。当这两个初始椭圆性的光束沿着短轴排列时， 当光束沿着短轴方向排列时，最终得到的光束（$z = 1.5m$）的形状由一个椭圆高斯决定，这个椭圆高斯的长轴跟两个原始光波中心的连接轴垂直。因此，单个光束的取向不是决定最终光束取向的因素，它决定了两光束中心的连接轴的取向。

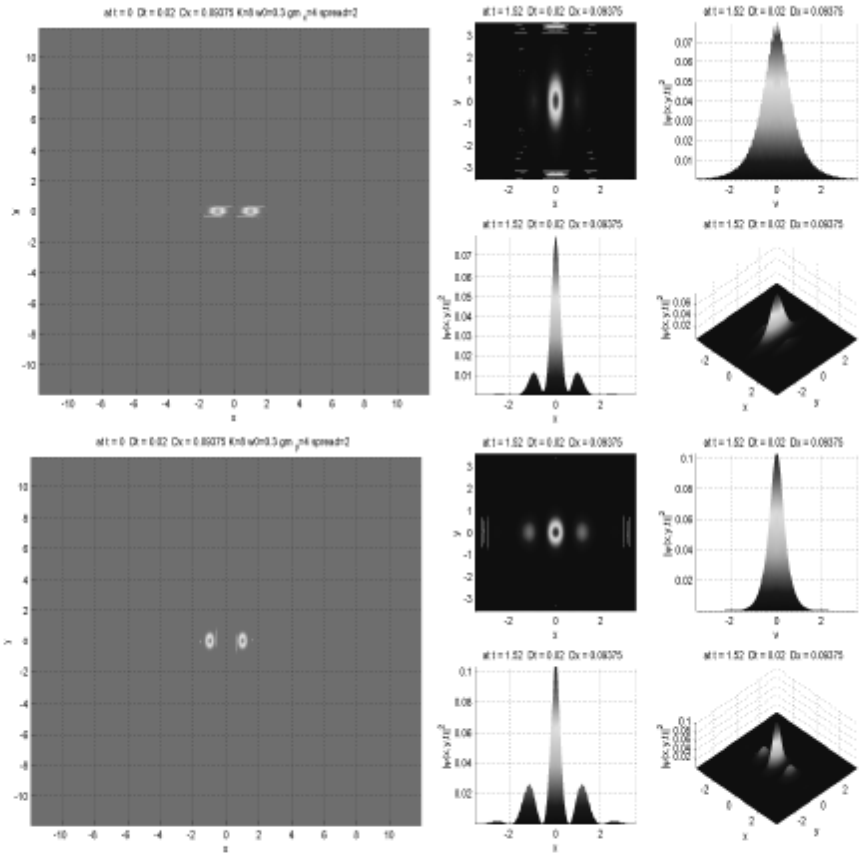

Figure 19: $|\psi(x,y,t)|$for two elliptical Gaussian beams, with beams' major axis parallel to (a) x轴(b) y轴 平行

图 19: $|\psi(x,y,t)|$两个椭圆高斯光束。首先光束的长轴跟(a) x轴(b) y轴 平行

When the beams are separated in the direction of the elliptical Gaussian, the center density resembles a right-shift of the center density when the beams are separated in the direction perpendicular to the Gaussians' major axis. It seems counterintuitive that the one with the higher initial value would be behind the one that was starting from near zero. Instead of growing from its higher initial value, it collapses and then rebuilds.

当初始时，两个光束沿椭圆高斯的长轴方向分离，中心密度代表了当这两个光束跟椭圆高斯的长轴垂直时，中心密度的向右位移。看起来这种情况是和直观不符合，因为有比较大的初始值的光波应该落后于初始值为0的光波。可是，在我们的结果中，它先是消减，然后重建，而不是从最大值开始增高。

4.3.2 Multiple Vortexing Gaussians多涡流性高斯

First, when the initial spins of the vortexes are in the same direction, the resulting beam contains two arcs and what resembles and behaves like a Gaussian. The Gaussian filaments well before the arcs do. The arcs take the shape of a vortexing pattern, but do not seem to actually vortex that much, as there does not appear to be a complete loop. The filaments on the arcs are generally and rather consistently about half the magnitude of the central filaments. This is for the conditions: $m_{(}charge) = 2$, with both shifted $\pm.75m$ in the $x = y$ direction. As can be observed from Figure 20, as time progresses, some filaments start to drift off and the arc shape becomes less and less recognizable. The filaments are still significant in intensity, but not as intense as before. There are also much fewer filaments. Dissipation happened faster for a longer time step.

首先，当两个涡流的旋转方向一样时，最终的光束包括两个弧线和那些看起来好像高斯形态的。高斯丝状比弧线的形成早得多。弧线形成涡流形态，但是并不那么明显，因为不能形成王政的回路。大部分弧线上的丝状有中心丝状的一半高。这种情况是当：$m_{(charge)} = 2$，它们在 $x = y$ 方向位移 $= +-0.75$。从图 20 也可以看出，随着时间推进，有些丝状开始离开弧线，弧线的形状越来越不清楚。丝状的强度还是很高的，可是没有以前的高。丝状也越来越少。时间步差越长，发散越快。

With similar spins, the initial beam was unbroken. The interference was constructive and thus the overlapping section was of greater magnitude than the rest of the double ring. In propagation however, the beam quickly bifurcates in the middle, causing what looks like asymmetric growth. The filaments only form in the area of overlap.

有相似的旋转方向，初始光束不分离。干扰开始建立，所以重叠部分比其他部分的大。但是，开始传播后，光束在中心很快的分叉，呈现非对称增长。丝状只形成在重叠部分。

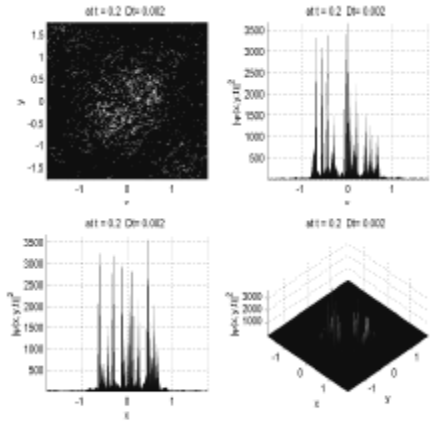

Figure 20: Two vortexing beams of opposite spin，Dt=0.002.

图 20: 两个反方向旋转涡流的光束，Dt=0.002.

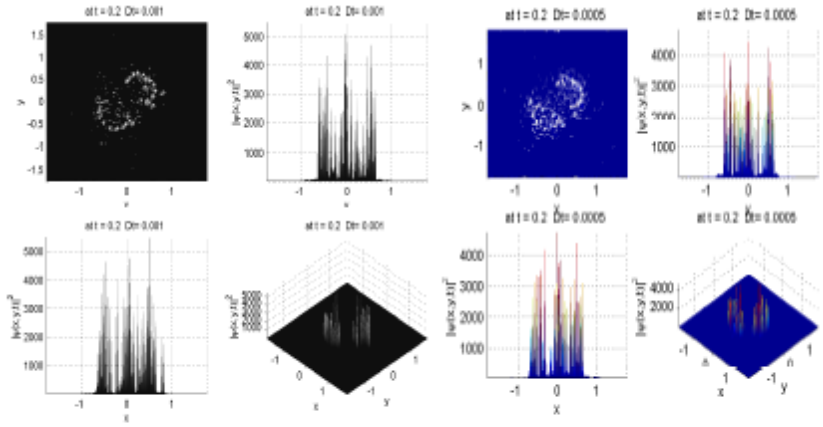

Figure 21: Two vortexing beams of opposite spin (a) Dt=0.001 (b) Dt=0.005

图 21: 涡流的光束有不同的旋转(a) Dt=0.001 (b) Dt=0.005。

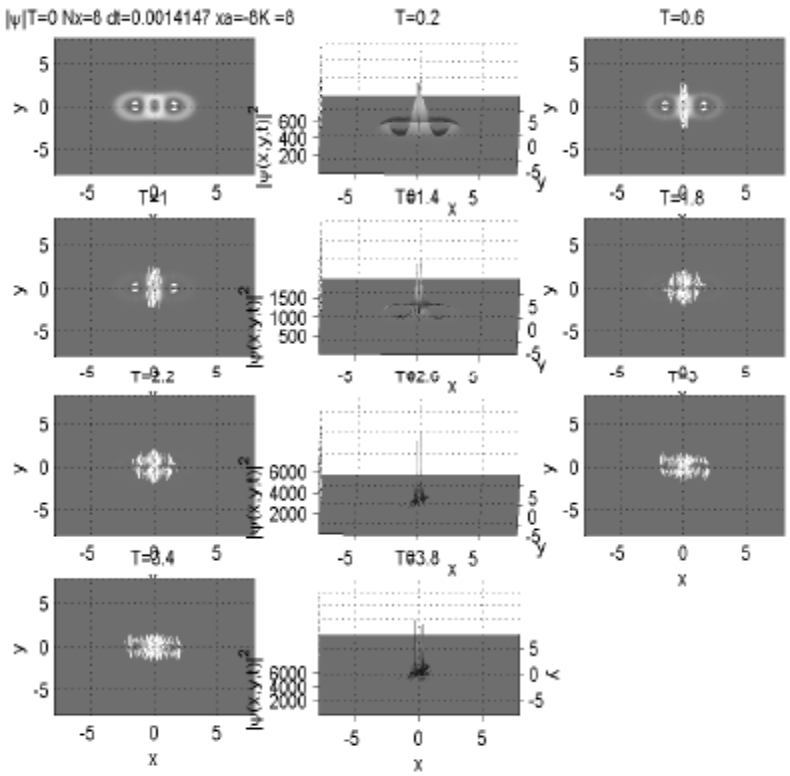

Figure 22: Vortexing beam with identical spin.

图 22: 涡流的光束有同一的旋转。

References 集合

[1] W. Bao and D. Jaksch, *An explicit unconditionally stable numerical method for solving damped nonlinear Schrödinger equations with a focusing nonlinearity*, SIAM J. Numer. Anal. 41 (2003), pp. 1406-1426.

[2] A. Vincotte and L. Bergé, *Atmospheric propagation of gradient-shaped and spinning femtosecond light pulses*, Physical D. 233 (2006), pp. 163-173.

[3] A. Vincotte and L. Bergé, χ^5 *susceptibility stabilizes the propagation of ultrashort laser pulses in air*, Physical Review A 70 (2004), pp.

Matthew Stein Academic Vita

449 Summit Drive
Pittsburgh, PA 15228

Mobile: 412-877-3438
Email: matthew.stein0@gmail.com

DEGREE

GPA: 3.73/4.0, 184 credits, 8 semesters.

Bachelor of Science in Mathematics (Honors) + Minor in Chemistry + Certificate of International Science
Applied Analysis Option in Mathematics
Pennsylvania State University, Schreyer Honors College (2005-2009)
Degree to be awarded on 2 August 2010
Honors Thesis: Time Splitting Sine Spectral Methods in Simulating Femtosecond Laser Propagation
Pritchard Fluid Mechanics Laboratory, AY2007-2008

Bachelor of Arts in Chinese (Honors) + Bachelor of Science in International Studies
Pennsylvania State University, Schreyer Honors College (2005-2009)
Degree to be awarded on 2 August 2010
Schreyer Honors College Summer 2007 Research Scholarship: Chinese Literature 2007

National University of Singapore: Education Abroad - Spring 2009 to Fall 2009
Honors Thesis: Time Splitting Sine Spectral Methods in Simulating Femtosecond Laser Propagation
Peking University: Collaborative mathematics research project – PSU–PKU - Summer 2008;
Chinese Thought and Culture – NUS University Scholars Programme – PKU Yuanpei College - Summer 2009
Soochow University: Furman-Soochow Summer Institute of Intensive Chinese - Summer 2007

RECENT EMPLOYMENT AND ACTIVITY HISTORY

Organizer – Conference Programs, Energy Carta – Energy and entrepreneurship NGO, Singapore, 2009
Organizer, Presidential campaign internship: Pittsburgh South Hills Office, 2008
Mathematics and Science Tutor – Summer 2006 to Present
Habitat for Humanity: Pennsylvania State University Chapter - 2006, 2007

AWARDS/ACHIEVEMENTS/SCHOLARSHIPS

Boren Scholarship: National Security Education Program, US Department of Defense AY2008-2009
Critical Language Scholarship**,** US Department of State 2007

ACADEMIC EXPERIENCE

Undergraduate Research Opportunities Programme for Science**,** NUS (SHC Honors Thesis) 2009
Pritchard Fluid Mechanics Laboratory, PSU AY2007-2008
Schreyer Honors College Summer 2007 Research Scholarship: Chinese Literature 2007

PROFESSIONAL CONFERENCES ATTENDED

Singapore International Energy Week and Clean Energy Expo Asia 2009
Energy Security Institute – Energy Security 2009
National Sustainability Conference – National University of Singapore – 2009
Solar Cell Seminar – Solaris and SERIS - Spring 2009
IYSECC - International Youth Summit on Energy and Climate Change – Tsinghua University - 2009
Sponsored Delegate: Energy Carta representative
Miracle Youth Conference 2009 – Universiti Putra Malaysia - AIESEC, Kuala Lumpur, Malaysia. 2009
Delegate, Speaker: "The Reasons Why: the tough realities and decisions our leaders face"
PKU ISO Beijing Global Issues Forum: "Foreign Corporations in China" Peking University International Seers Organization 2009